Research Journal of Recent Sciences _____ ISSN 2277-2502
Vol. **6(2),** 1-9, February **(2017)** *Res. J. Recent Sci.*

Effect of temperature on the structural, morphological and magnetic properties of magnesium ferrite nanoparticles

Lavanya Khanna* **and S.K. Tripathi**
Department of Physics, Panjab University, Chandigarh-160014, India
lavanshya@yahoo.co.in

Available online at: www.isca.in, www.isca.me
Received 29th November 2016, revised 28th January 2017, accepted 30th January 2017

Abstract

In the present paper, magnesium ferrite nanoparticles were synthesized by conventional sol–gel method. The as-synthesized material was calcined at different temperatures and their structural, magnetic, FTIR, morphological and compositional analyses were studied. XRD patterns revealed formation of cubic structured magnesium ferrite nanoparticles. With the increase in calcination temperature, the crystallite size increased and crystallinity improved. No peaks corresponding to any impurity or additional phases were detected; this was also confirmed by the FTIR spectra. With increase in the temperature, a gradual disappearance of C-H, hydroxylate and carboxylate groups occurred, while Fe-O bond became prominent. The magnetic analysis done by VSM revealed superparamagnetic behavior of the calcined nanoparticles. With increase in temperature, magnetic saturation, coercivity, remanent magnetization and magnetic squareness value increased, owing to improved crystallization and bigger particle size. Considering biomedical application, this is an undesired feature as more the squareness value, lesser is the superparamagnetic character. The sample calcined at 500°C was found to be the most suitable for carrying out further investigations. Its morphological and compositional analysis revealed its spherical agglomerated formation with the desired elemental composition. In vitro cytotoxicity test on HaCaT cells using MTT (3-(4, 5-Dimethylthiazol-2-yl)-2, 5- diphenyltetrazolium bromide, a tetrazole) assay revealed the concentration-dependent cell-viability of the synthesized magnesium ferrite nanoparticles. The spherical formation, superparamagnetism and cell-viability (at lower concentrations) allows for its successful application in biomedicine.

Keywords: Magnesium ferrite nanoparticles, Superparamagnetic, Spherical nanoparticles, Biomedical applications, Spinel ferrites.

Introduction

Magnetic nanoparticles (MNPs) have been extensively explored for varied applications such as biological sensors, contrast agents in magnetic resonance imaging, decontamination of biological solutions, targeted drug delivery, hyperthermia and magnetic separation[1-3]. The basic requirements for materials to be used in the above mentioned applications are i. size in nanometers ii. good dispersibility in suspensions iii. superparamagnetic behavior and iv. non-toxicity. All these properties have been investigated in materials such as Fe_3O_4[4–6], $NiFe_2O_4$[4,7,8], $CaFe_2O_4$[9-12], $KFeO_2$[13-15], $CoFe_2O_4$[16-18], $MnFe_2O_4$[19,20] and $ZnFe_2O_4$[4] nanoparticles. Although, ferrites of Ni, Mn, Co, Zn exhibit excellent magnetic properties, their inherent toxicity elevates worries on their biocompatibility and successful application in biomedicine field.

Therefore, it is essential to utilize such a material which does not have any inherent toxicity threat associated with it, such as magnesium. Among ferrites, magnesium ferrite is an interesting spinel ferrite material because in it, magnetic couplings of Fe cations are solely responsible for existence of magnetic moment, where presence of non-magnetic Mg^{2+} metal ions reduces the overall moment[3]. Due to this, its magnetic anisotropy is lesser as compared to other spinel ferrites, in which metal cations have larger magnetic moments[3]. It is very well-known that the magnetic properties of spinel ferrites are strongly dependent on the distribution of the different cations placed at A and B sites; this is also related to the thermal history, shape and size of the nanoparticles[21]. Magnesium ferrite nanoparticles possess typical superparamagnetic properties, which is one of the major necessities for biomedical applications. Superparamagnetic materials exhibit zero coercivity and zero retentivity on removal of external magnetic field.

This feature makes them highly desirable for biomedical applications where a strict dose-dependent and time-dependent protocol is followed for treatment of dreadful diseases. The formation, structural, magnetic and biocompatibility studies of magnesium ferrite nanoparticles have been reported by various researchers[22-32].

The present work reports about the synthesis of magnesium ferrite nanoparticles using sol-gel method. The synthesized nanoparticles were calcined at different temperatures. The obtained samples were studied using X-ray diffraction (XRD), Scanning Electron Microscope (SEM) with energy dispersive spectroscope (SEM-EDS), Field- emission Scanning Electron

Microscope (FE-SEM), Fourier infrared spectroscope (FTIR) and Vibrating sample magnetometer (VSM). The concentration-dependent cell viability test was determined by MTT (3-(4, 5-dimethylthiazol-2yl)-2, 5-diphenyl tetrazolium bromide) assay. Their structural, morphological, magnetic and FTIR behavior w.r.t. temperature have been analyzed and reported.

Materials and methods

Materials: All the chemicals utilized in the synthesis process were of AR grade. Magnesium nitrate ($Mg(NO_3)_2.6H_2O$) was purchased from sdfine chem ltd, India, Ferric nitrate ($Fe(NO_3)_3.9H_2O$) from Loba chemie, citric acid ($C_6H_8O_7.H_2O$) from Fisher Scientific and ethylene glycol from central drug house (CDH) ltd, New Delhi, India. The chemicals were used without any further purification.

Synthesis of magnesium ferrite nanoparticles: Standard so-gel method was used for the chemical route synthesis of magnesium ferrite nanoparticles[33]. 1M solution of magnesium nitrate was mixed with 2M solution of ferric nitrate and stirred magnetically. 2M citric acid solution and 10 ml of ethylene glycol was added. This solution was continually mixed on the magnetic stirrer at 90ºC. The basis of this process is ethylene glycol mediated metallic citrate polymerization[33]. Metal nitrates used in this process act as soluble cation source as well as oxidant[34]. Citric acid provides fuel for combustion process and also acts as a chelating mediator for complex-formation with metal ions.

Also, it prevents the formation of precipitates of hydroxylates[34] and serves as non-polymeric space filler in order to control the size and porous nature of nanoparticles[35]. It can be easily removed by heating, without affecting the synthesized product[35]. Constant stirring led to formation of a viscous gel which began to froth as the water molecules were removed from the solution. On further heating, the solution became more viscous, then a brown gel was formed and finally dehydrated gel was obtained which persistently burned on its own until a brown colored powder was formed. Thus, indicating the complete burning up of the whole citrate complex. The washing was done in ethanol using centrifuge.

It was kept in vacuum oven at 80ºC till it completely dried up. The obtained powder was calcined at 300ºC (Mg3), 500ºC (Mg5), 700ºC (Mg7), 900ºC (Mg9), for 3 h each. Following is the chemical reaction of the synthesis process:

$$9Mg(NO_3)_2.6H_2O+18Fe(NO_3)_2.9H_2O+14C_6H_8O_7.H_2O\rightarrow 9MgFe_2O_4+286H_2O+27N_2+84CO_2 \quad (1)$$

Characterizations: Morphological and crystalline properties: The morphology and composition of synthesized nanoparticles (NPs) was analyzed by scanning electron microscope (SEM; JSM, 6510 LV, JEOL (U.S.A) and energy-dispersive spectroscopy, EDS, Oxford), coating with gold was done using JEOL, JFC sputter coater and field emission scanning electron microscope (FE-SEM, Hitachi S4300 SE/N). The crystalline properties were studied by X-ray diffraction (Rigaku, Mini Flex 600).

Fourier transform infrared spectroscopy: The FT-IR spectra (4000–400 cm^{-1}) of the powdered nanoparticles pressed into 13 mm thick KBr pellets were recorded on Perkin Elmer-Model RZX.

Magnetic analysis: The magnetic properties and parameters of the synthesized nanoparticles were obtained on vibrating sample magnetometer (LakeShore 7404).

Cell Viability assay: Cytotoxicity of the synthesized nanoparticles was obtained by MTT (3-(4, 5-dimethylthiazol-2yl)-2,5-diphenyl tetrazolium bromide) assay on HaCaT cells (3×10^4) at various concentrations (µg/ml) from Department of Biophysics, Panjab University, Chandigarh[36].

Results and discussion

Crystalline analysis: The XRD patterns at room temperature were obtained in the angle range of 10°– 90° with step size of 0.02. Figure-1 shows the X-ray patterns of the as-synthesized nanoparticles as well as nanoparticles calcined at 300°C (Mg3), 500°C (Mg5), 700°C (Mg7), 900°C (Mg9). In the as-synthesized sample, no peaks were observed, indicating its lack of crystallinity. It is observed that uncalcined sample is mainly amorphous in nature without any presence of nitrate, as also shown in FTIR spectrum (Figure-2). Even nanoparticles calcined at 300°C, did not attain complete crystallinity, only weak peaks of very low intensity have been observed. In the XRD patterns of samples calcined at 500°C (Mg5), 700°C (Mg7), 900°C, all the observed peaks correspond to the cubic structure having space group: Fd3m(227), JCPDS Card No. 73-2211, of $MgFe_2O_4$. Six major diffraction peaks corresponding to (2 2 0), (3 1 1), (4 0 0), (4 2 2), (5 1 1) (4 4 0) have been observed.

The crystallite size corresponding to the prominent highest peak broadening of plane (3 1 1) was calculated using Debye Scherrer formula, as follows.

$$d = \frac{k\lambda}{\beta Cos\theta} \quad (2)$$

Where: d is the crystallite size, k = 0.9 (correction factor), β is the full width half maximum (FWHM) of the most intense peak (3 1 1), λ is Cu target wavelength i.e. 1.5406 Å and θ corresponds to Bragg angle. The crystallite size and lattice parameter value *a* (Å), as calculated have been tabulated in Table-1. It can be well - observed that with increase in calcination temperature, crystallinity of the samples improved and also their size increased, thus indicating the temperature sensitivity of the synthesized nanoparticles. No peaks corresponding to any impurity or additional phases were detected.

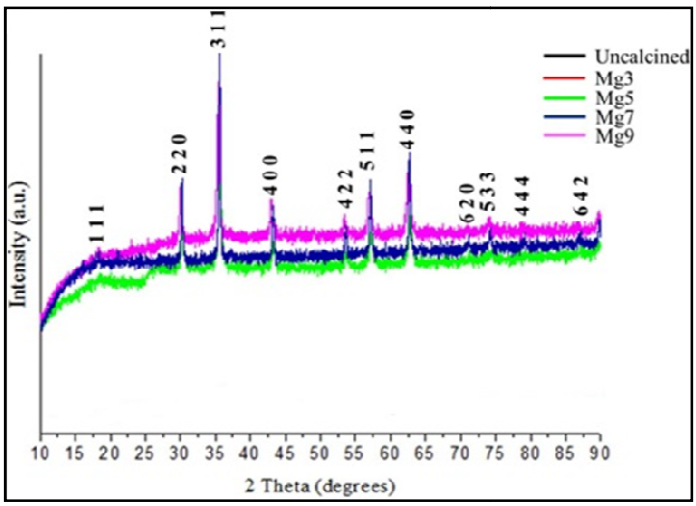

(a)

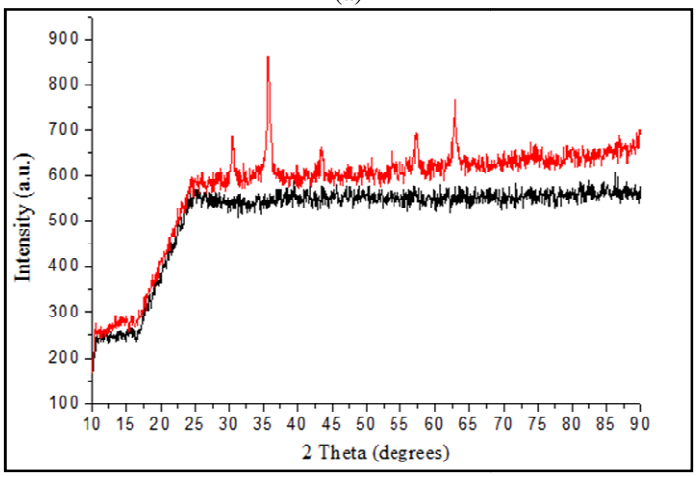

(b)

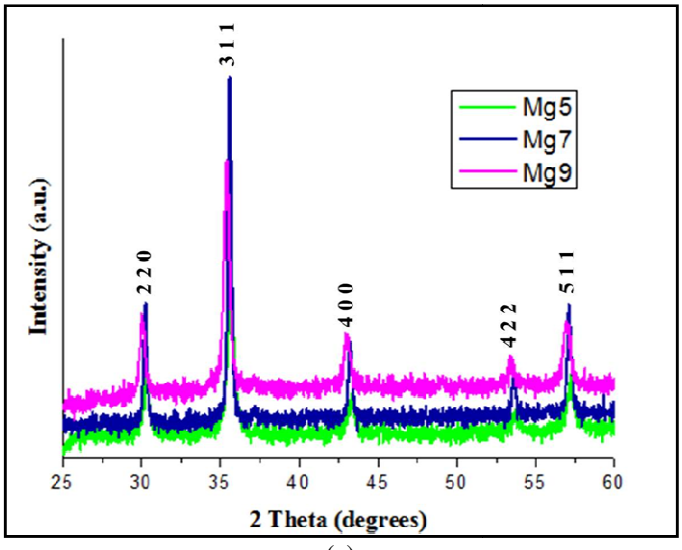

(c)

Figure-1: XRD patterns of (a) all samples (b) uncalcined at calcined at 300°C (c) XRD patterns of the nanoparticles calcined at 500°C, 700°C and 900°C in the angle range of 25°–60°.

Table-1: Crystallite sizes (nm) estimated by Scherrer's formula and unit cell parameter.

Sample	Crystallite size (nm)	Unit cell parameter, *a(Å)* (Calculated)	Unit cell parameter, *a(Å)* (Theoretical)	Difference
Mg5	18	6.003	8.366	2.363
Mg7	23	7.794	8.366	0.572
Mg9	37	12.570	8.366	4.204

FT-IR analysis: FT-IR spectra (4000–400 cm^{-1}) of the as-synthesized nanoparticles and calcined nanoparticles were recorded and are shown in Figure-2. In all the graphs, the broad absorption ~3400 cm^{-1} represents the characteristic stretching vibration of hydroxylate (O–H) group due to absorption of water molecules. Also, it can be well-observed that no distinctive bands corresponding to nitrate ions have been detected, as shown in XRD pattern as well (Figure-1).

This indicates that during heating of the gel, oxidation–reduction reaction occurred in which carboxyl ions acted as reducing agent and nitrate ions as oxidizers. In the uncalcined sample, peaks at 1610 cm^{-1} and 1393 cm^{-1} are allotted to asymmetrical as well as symmetrical stretching vibration of carboxylate (O–C-O), respectively[26]. Peaks at 1251 cm^{-1} and 1070 cm^{-1} correspond to asymmetrical and symmetrical stretching vibration of C–O–C group[26]. Peaks obtained at 856 cm^{-1}, 689 cm^{-1} and 641 cm^{-1} correspond to deformation vibration of the C–H group[26]. The small peak at 466 cm^{-1} corresponds to stretching vibration of metal-oxygen bond (Fe-O), denoting formation of a Fe- citrate complex[9-15].

In all the FTIR spectra of the calcined samples, gradual disappearance of C-H, hydroxylate and carboxylate groups can be well-observed. In the sample calcined at 300°C, the split of the carboxylate group has reduced significantly and with increase in the temperature further, it reduces completely. Also, the peaks of C-O-C and C-H group reduce significantly with increase in temperature, while the peaks of metal-oxygen (Fe-O) group become prominent. The observed peak around 2400 cm^{-1} is assigned to the CO_2 present in the atmosphere. Generally, in ferrites, peaks in the wave number region (500–600 cm^{-1}) are allocated to the tetrahedral complexes, while peaks appearing in the wave number region (400–450 cm^{-1}) are assigned to the octahedral complexes[3].

So, it can be concluded that peaks in these regions are identified to be the characteristic absorption peaks of magnesium ferrite nanoparticles. Description of the peaks obtained in spectra of all samples has been tabulated in Table-2.

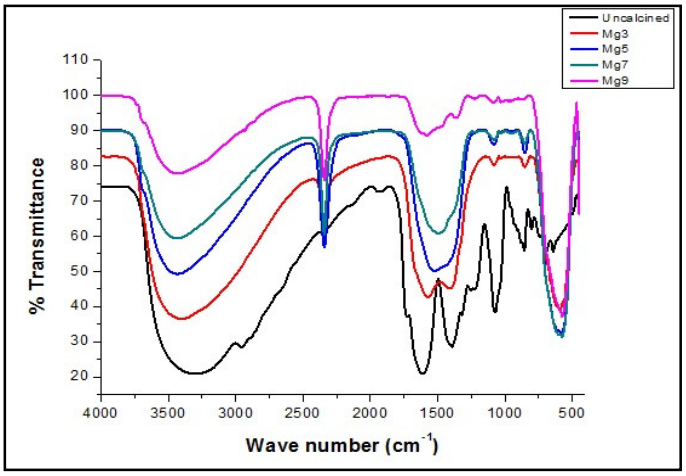

Figure-2: FTIR spectra of magnesium ferrite nanoparticles (uncalcined and calcined at different temperatures).

Magnetic analysis: VSM was performed, as shown in Figure-3, to examine the magnetic properties of all the synthesized nanoparticles. M-H curve of the uncalcined sample, Figure-3(a), indicates its poor crystallization. This is also well- reflected in the XRD pattern (Figure-1(a)), resulting in negligible magnetization and zigzag M-H curve. Calcining the samples at 300°C, 500°C, 700°C and 900°C led to formation of superparamagnetic nanoparticles.

The trends of saturation magnetization, remanent magnetization and coercivity have been shown in Figure-3 (b). It can be well-observed that saturation magnetization, retentivity and coercivity increase with increase in temperature. The magnetization of samples calcined at 300°C, 500°C, 700°C and 900°C are 11.41 emu/g, 21.66 emu/g, 24.04 emu/g, 26.06 emu/g. This is attributed to surface disorder, cation distribution and defects occurring due to size reduction in the nanoparticles[26].

The increase in saturation magnetization with temperature occur because of improvement in crystallinity and decrease of oxygen vacancies. As also observed in the FTIR studies (Figure-2), the metal-oxygen (Fe-O) band becomes prominent on increasing the temperature, thereby reducing the oxygen vacancies. This strengthening of the Fe-O group results in improvement of the magnetic saturation value and hence on increasing the calcination temperature, MS value increases. However, the other consequence of this increase is the significant increase of the particle size, as depicted in the XRD patterns (Figure-1) and Table-1.

The coercivity and crystallite size of samples calcined at 500°C, 700°C and 900°C are 29.35 Oe, 72.49 Oe, 87.39 Oe and 18 nm, 23 nm, 37 nm, respectively. Particle size growth with temperature has resulted in coercivity enhancement. It is well-known that spin of the ions present at A and B sites, oppositely magnetize the sub-lattices. The ensuing magnetic moment equals to the variation between these two[9,34,37].

Table-2: Description of FT-IR spectra of magnesium ferrite nanoparticles uncalcined and calcined at all temperatures.

Sample	IR region or bands (cm−1)	Descriptions
Uncalcined	3315	*v*(OH) stretch
	1610	*v*(O-C=O) asymmetrical stretch
	1393	*v*(O-C=O) symmetrical stretch
	1251	*v*(C-O-C) asymmetrical stretch
	1070	*v*(C-O-C) symmetrical stretch
	856, 689, 641	*v*(C-H) deformation vibrations
	466	*v*(Fe-O) stretch
Mg3	3407	*v*(OH) stretch
	2339	*v*(CO_2) stretch
	1570	*v*(O-C=O) asymmetrical stretch
	1413	*v*(O-C=O) symmetrical stretch
	1082	*v*(C-O-C) symmetrical stretch
	854, 690	*v*(C-H) deformation vibrations
	590	*v*(Fe-O) stretch
Mg5	3432	*v*(OH) stretch
	2342	*v*(CO_2) stretch
	1526	*v*(O-C=O) asymmetrical stretch
	1084	*v*(C-O-C) symmetrical stretch
	850	*v*(C-H) deformation vibrations
	573, 469	*v*(Fe-O) stretch
Mg7	3432	*v*(OH) stretch
	2341	*v*(CO_2) stretch
	1497	*v*(O-C=O) asymmetrical stretch
	1080	*v*(C-O-C) symmetrical stretch
	851	*v*(C-H) deformation vibrations
	576	*v*(Fe-O) stretch
Mg9	3433	*v*(OH) stretch
	2340	*v*(CO_2) stretch
	1577	*v*(O-C=O) asymmetrical stretch
	575	*v*(Fe-O) stretch

Using the following equation, the value of nB (M_S per formula unit in Bohr magneton) has been calculated from the M-H curve:

$$nB = \frac{MW \times Ms}{5585} \quad (3)$$

Where: MW corresponds to the molecular weight of the compound ($MgFe_2O_4$) and MS is the saturation magnetization. The values of magnetic saturation (MS), remanent magnetization (MR), coercivity (HC), magnetic squareness (MR/MS ratio) and magneton number, as obtained, have been tabulated in Table-3. The squareness value corresponding to non- interacting superparamagnetic nanoparticles is 0.5, while for interacting superparamagnetic particles, reduction in dipolar interaction introduces demagnetizing effects which further decrease the coercivity and magnetic squareness values[38]. Squareness value corresponding to superparamagnetic behavior is 0.1. It means greater than 90% magnetism is lost on abolition of external magnetic field[39]. The squareness value, as obtained for Mg5, Mg7 and Mg9 are 0.045, 0.108 and 0.153, respectively. All the samples exhibit superparamagnetism but high level of coercivity and retentivity in Mg7 and Mg9 sample is an undesired feature, thereby making Mg5 the most suitable sample for future investigations.

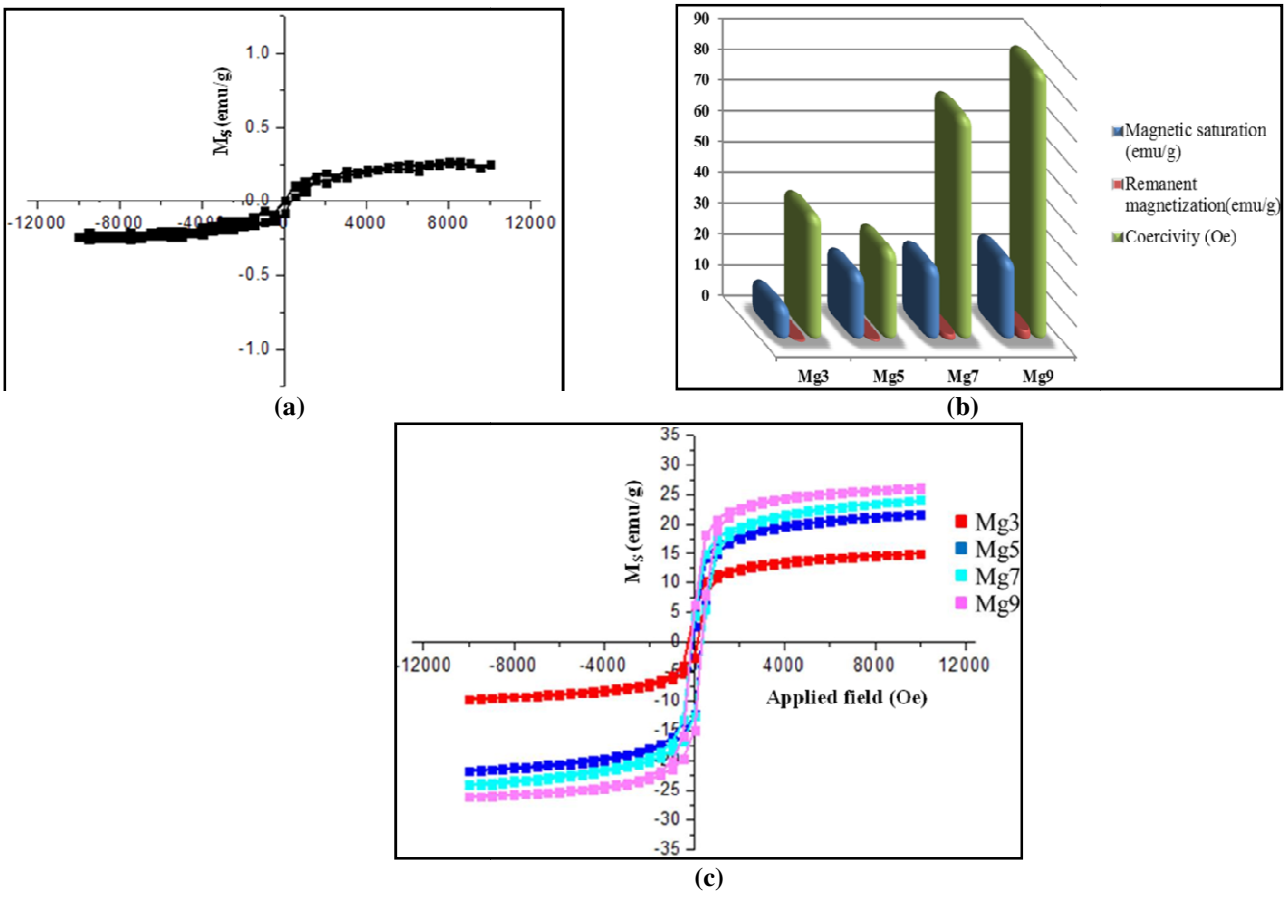

Figure-3: M–H curve of magnesium ferrite nanoparticles (a) uncalcined (b) calcined at all temperatures (c) Magnetic parameters of the calcined samples.

Table-3: Hysteresis parameters for all calcined nanoparticles

Sample name	Saturation magnetization (MS) (emu/g)	Remanence (MR) (emu/g)	Coercivity (HC) (Oe)	Squareness (MR/MS)	Magneton Number (nB)
Mg3	11.41	0.71	40.46	0.062	0.29
Mg5	21.66	0.98	29.35	0.045	0.55
Mg7	24.04	2.61	72.49	0.108	0.62
Mg9	26.06	3.98	87.39	0.153	0.67

Morphological and compositional analysis: SEM and EDS studies were executed in order to comprehend the particulars of morphology of synthesized magnesium ferrite nanoparticles, calcined at 500°C. Figure-4 shows the SEM micrograph at different magnifications and EDS pattern along with its respective table depicting the atomic % values of the elements observed. The image shows spherical shaped agglomerated particles in the nano-metric region. High surface energy of the nanoparticles results in agglomeration; this feature is inherently associated with them. Figure-4 (d, e) shows the SEM micrograph of the nanoparticles calcined at 900ºC. In it, rod shaped formation along with spherical nanoparticles can be well-observed. Therefore, a mixed morphology of the synthesized nanoparticles makes it unwanted for biomedical applications. Decuzzi et al. have reported that spherical nanoparticles exhibit lesser cytotoxicity as compared to other shaped nanostructures *(They produced models suggesting that spherical nanoparticles displayed more diffusion rates with increased concentration at the centre of a blood vessel. This resulted in limited interactions with endothelial cells, which is a thin layer of cells that outlines the inner surface of all blood vessels. This is present in the whole circulatory system, thus extending the circulation of any drug delivery agent in the body)*[40]. For targeted drug delivery applications, it is essential to have a narrow size range as that would correspond to identical possibility of magnetic susceptibility and drug dosage, overall[9, 18]. The table shown in Figure-4(c) exhibits the stoichoimetric formation of the synthesized magnesium ferrite nanoparticles.

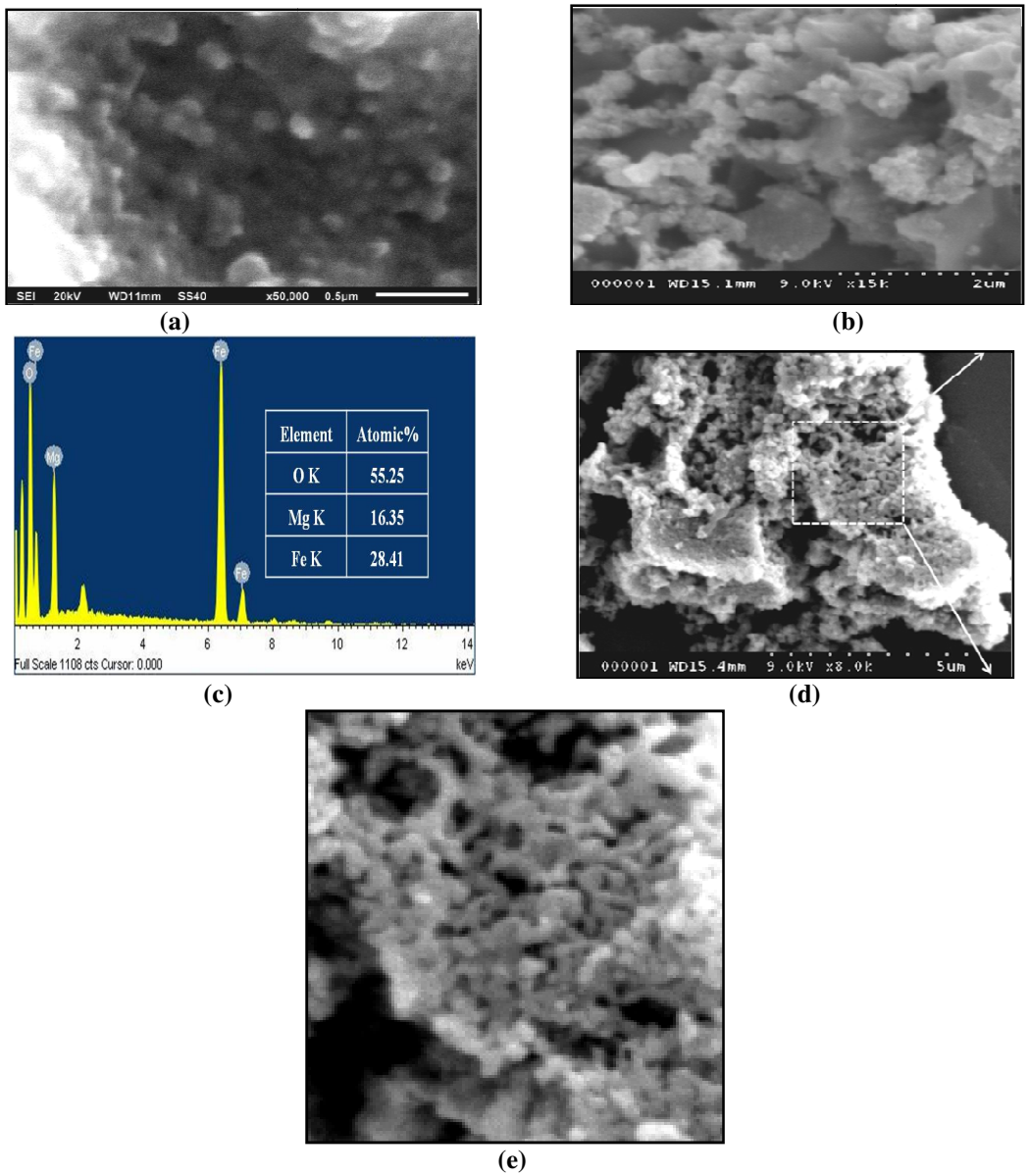

Figure-4: (a, b) SEM and FE-SEM micrograph at different magnifications and (c) EDS along with table depicting elemental composition (d) FE-SEM micrograph of Mg9 (e) Magnified image of the dotted box.

Cell-viability analysis: In Figure-5, the concentration dependent cell-viability of calcined magnesium ferrite nanoparticles (500ºC) has been shown. It has been determined using the formula, as follows:

$$Cell-viability(\%) = \frac{Isample}{Icontrol} \times 100 \quad (4)$$

where, I(sample) corresponds to the absorbance of nanoparticles treated wells and I(control) corresponds to the absorbance of the control without any nanoparticle treatment[41]. Using Equation 4, the cell viabilities at 5, 25, 50, 100, 250, 500 mg/ml, have been calculated to be 92.4%, 89.8%, 59.5%, 59.5%, 45.1%, 18.2% respectively. With increase in concentration, the cell viability decreases dramatically i.e. a substantial cell death occurs at higher concentration. Tomitaka et al. explained this behavior, stating that nanoparticles first stick to the cell surface, then are internalized by endocytosis and eventually get accrued in digestive vacuoles[4, 12]. Therefore, cell death at higher concentrations is most probably triggered by particle overload[4,12]. Mahmoudi et al. have explained that interaction of nanoparticle with protein corona of the cell determines its toxicity. On interaction, owing to some hostile modifications in the protein configuration, the proteins get denatured, thereby leading to new immune response[42]. The spherical formation, superparamagnetism and cell- viability (at lower concentrations) allows for its positive feasibility in biomedicine. Further studies for its applications in targeted drug delivery are in process and significant outcomes can be well-anticipated.

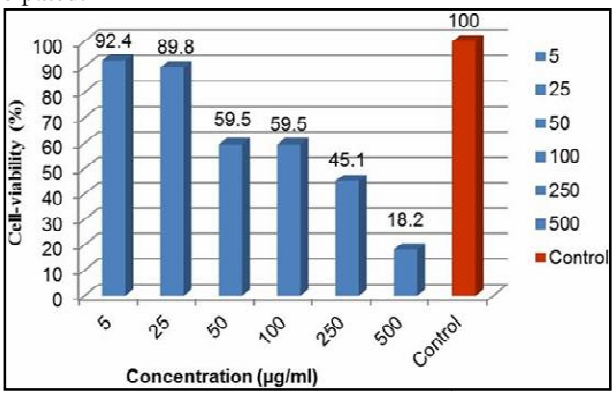

Figure-5: Mean cell-viability (%) of magnesium ferrite nanoparticle calcined at 500ºC.

Conclusion

The present paper reports about synthesis and temperature-dependent characterization of magnesium ferrite nanoparticles for biomedical applications. XRD patterns reveal the formation of cubic structure of $MgFe_2O_4$. As the temperature increases, an increase in crystallite size occurs, with improved crystallinity. No additional peaks pertaining to any impurity or additional phases have been detected. The presence of characteristic peaks of the desired elements in the FTIR spectra also confirms the successful formation of magnesium ferrite nanoparticles, without any impurity. With increase in temperature, a gradual disappearance of C-H, hydroxylate and carboxylate groups occurred, whereas Fe-O bond strengthened. Superparamagnetic behavior of the calcined nanoparticles has been shown in the M-H curves. Magnetic saturation, coercivity, remanent magnetization and magnetic squareness value increase with temperature due to improved crystallization and bigger particle size. Considering the requirements for biomedical application, sample calcined at 500°C (Mg5) is recommended to be the most appropriate. Its spherical formation and stoichiometric compositional analysis has been observed in the SEM micrograph and EDS analysis, respectively. MTT assay using HaCaT cell lines of Mg5 sample displayed its concentration-dependent cell-viability. More cell death occurred at higher concentration, owing to particle overload and shortage of media. Its spherical formation, superparamagnetism, cell-viability makes it a feasible candidate for biomedical applications.

Acknowledgement

Dr. Lavanya Khanna gratefully acknowledges University Grants Commission, Government of India, New Delhi, India for awarding her Dr. D. S. Kothari Postdoctoral Fellowship to carry out this research work. The author is deeply thankful to Dr. Simranpreet, Assistant professor, Department of Biophysics, Panjab University, Chandigarh for obtaining the MTT assay results.

References

1. Gupta A.K. and Gupta M. (2005). #Synthesis and surface engineering of iron oxide nanoparticles for biomedical applications.# *Biomater,* 26(18), 3995–4021.

2. Pankhurst Q.A., Connolly J., Jones S.K. and Dobson J. (2003). #Applications of magnetic nanoparticles in biomedicine.# *J. Phys. D: Appl. Phys.* 36(13), R167–R181.

3. Khot V.M., Salunkhe A.B., Phadatare M.R. and Pawar S.H. (2012). #Formation, microstructure and magnetic properties of nanocrystalline MgFe2O4.# *Mater. Chem. Phy.* 132(2), 782– 787.

4. Tomitaka A., Hirukawa A., Yamada T., Morishita S. and Takemura Y. (2009). #Biocompatibility of various ferrite nanoparticles evaluated by in vitro cytotoxicity assays using HeLa cells.# *J. Magn. Magn. Mater.,* 321(10) 1482–1484.

5. Zhang J., Rana S., Srivastava R.S. and Misra R.D.K. (2008). #On the chemical synthesis and drug delivery response of folate receptor-activated, polyethylene glycol-functionalized magnetite nanoparticles.# *Acta Biomater*, 4(1), 40–48.

6. Yallapu M.M., Othman S.F., Curtis E.T., Gupta B.K., Jaggi M. and Chauhan S.C. (2011). #Multi- functional magnetic nanoparticles for magnetic resonance imaging and cancer

therapy.# *Biomaterials,* 32(7), 1890–1905.

7. Yin H., Too H.P. and Chow G.M. (2005). #The effects of particle size and surface coating on the cytotoxicity of nickel ferrite.# *Biomaterials.* 26(29), 5818–5826.

8. Rana S., Gallo A., Srivastava R.S. and Misra R.D.K. (2007). #On the suitability of nanocrystalline ferrites as a magnetic carrier for drug delivery: functionalization, conjugation and drug release kinetics.# *Acta Biomaterialia,* 3(2), 233–242.

9. Khanna L. and Verma N.K. (2013). #Size-dependent magnetic properties of calcium ferrite nanoparticles.# *J. Magn.Magn. Mater.,* 336, 1-7.

10. Khanna L. and Verma N.K. (2013). #PEG/$CaFe_2O_4$ nanocomposite: Structural, morphological, magnetic and thermal analyses.# *Physica B,* 427, 68–75.

11. Khanna L. and Verma N.K. (2014). #Biocompatibility and superparamagnetism in novel silica/$CaFe_2O_4$ nanocomposite.# *Mater. Lett.,* 128, 376-379.

12. Khanna L. and Verma N.K. (2013). #Synthesis, characterization and invitro cytotoxicity study of calcium ferrite nanoparticles.# *Mater. Sci. Semicond. Process.*, 16(6), 1842–1848.

13. Khanna L. and Verma N.K. (2015). #Study on novel, superparamagnetic and biocompatible PEG/$KFeO_2$ nanocomposite.# *J. Appl. Biomed.,* 13(1), 23-32.

14. Khanna L. and Verma N.K. (2013). #Silica/potassium ferrite nanocomposite: Structural, morphological, magnetic, thermal and in vitro cytotoxicity analysis.# *Mater. Sci. Eng. B,* 178(18), 1230-1239.

15. Khanna L. and Verma N.K. (2014). #Synthesis, characterization and biocompatibility of potassium ferrite nanoparticles.# *J. Mater. Sci. Tech.,* 30(1), 30-36.

16. Mohapatra S., Rout S.R., Maiti S., Maiti T.K. and Panda A.B. (2011). #Monodisperse mesoporous cobalt ferrite nanoparticles: synthesis and application in targeted delivery of antitumor drugs.# *J. Mater. Chem.*, 21(25), 9185-9193.

17. Baldi G., Bonacchi D., Franchini M.C., Gentili D., Lorenzi G., Ricci A. and Ravagli C. (2007). #Synthesis and coating of cobalt ferrite nanoparticles: a first step toward the obtainment of new magnetic nanocarriers.# *Langmuir* 23(7), 4026–4028.

18. Rana S., Philip J. and Raj B. (2010). #Micelle based synthesis of cobalt ferrite nanoparticles and its characterization using Fourier transform infrared transmission spectrometry and thermogravimetry.# *Mater. Chem. Phys.*, 124(1), 264–269.

19. Yang H., Zhang C., Shi X., Hu H., Du X., Fang Y., Ma Y., Wu H. and Yang S. (2010). #Water-soluble superparamagnetic manganese ferrite nanoparticles for magnetic resonance imaging.# *Biomater.,* 31(13), 3667–3673.

20. Leung K.C.F. and Wang Y.X.J. (2010). #Nanowires Science and Technology in N. Lupu (Ed.).# *InTech, Croatia*, 331–344.

21. Ferreira da Silva M.G. and Valente M.A. (2012). #Magnesium ferrite nanoparticles inserted in a glass matrix— Microstructure and magnetic properties.# *Mater. Chem. Phy.,* 132(2), 264-272.

22. Foroughi F., Hassanzadeh-Tabrizi S.A. and Bigham A. (2016). #In situ microemulsion synthesis of hydroxyapatite-$MgFe_2O_4$ nanocomposite as a magnetic drug delivery system.# *Mater. Sci. Eng. C,* 68, 774-779.

23. Nedim Ay A., Konuk D. and Karan B.Z. (2011). #Magnetic nanocomposites with drug-intercalated layered double hydroxide shell supported on commercial magnetite and laboratory-made magnesium ferrite core materials.# *Mater. Sci.Eng. C* 31(5), 851–857.

24. Nonkumwong J., Pakawanit P., Wipatanawin A., Jantaratana P., Ananta S. and Srisombat L. (2016). #Synthesis and cytotoxicity study of magnesium ferrite-gold core-shell nanoparticles.# *Mater. Sci. Eng. C,* 61,123–132.

25. Hyun S.W., Kim H.J., Park C.S., Kang K.S. and Kim C.S. (2009). #Synthesis and Size Dependent Properties of Magnesium Ferrites.# *IEEE Transactions on Magnetics,* 45(6), 2551-2553.

26. Huang Y., Tang Y., Wang J. and Chen Q. (2006). #Synthesis of $MgFe_2O_4$ nanocrystallites under mild conditions.# *Mater. Chem. Phy.,* 97(2), 394-397.

27. Hussein S.I., Elkady A.S., Rashad M.M., Mostafa A.G. and Megahid R.M. (2015). #Structural and magnetic properties of magnesium ferrite nanoparticles prepared via EDTA-based sol–gel reaction.# *J. Magn. Magn. Mater.*, 379, 9-15.

28. Chandradass J. and Kim K.H. (2011). #Solvent effects in the synthesis of $MgFe_2O_4$ nanopowders by reverse micelle processing.# *J. Alloys Compds.,* 509(5), L59-L62.

29. Pradeep A., Priyadharsini P. and Chandrasekaran G. (2008). #Sol– gel route of synthesis of nanoparticles of $MgFe_2O_4$ and XRD, FTIR and VSM study.# *J. Magn. Magn. Mater.*, 320(21), 2774–-2779.

30. Das H., Sakamoto N., Aono H., Shinozaki K., Suzuki H. and Wakiya N. (2015). #Investigations of superparamagnetism in magnesium ferrite nano-sphere synthesized by ultrasonic spray pyrolysistechnique for hyperthermia application.# *J. Magn. Magn. Mater.*, 392, 91–100.

31. Chandradass J., Jadhav A.H., Kim K.H. and Kim H. (2012). #Influence of processing methodology on the structural and magnetic behavior of $MgFe_2O_4$ nanopowders.# *J. Alloys Compds.,* 517, 164-169.

32. Sivakumar N., Narayanasamy A., Greneche J.M., Murugaraj R. and Lee Y.S. (2010). #Electrical and magnetic behaviour of nanostructured MgFe2O4 spinel ferrite.# J. *Alloys Compd*., 504(2), 395-402.

33. Candeia R.A., Bernardi M.I.B., Longo E., Santos I.M.G. and Souza A.G. (2004). #Synthesis and characterization of spinel pigment $CaFe_2O_4$ obtained by the polymeric precursor method.# *Mater. Lett.,* 58(5), 569-572.

34. Thant A.A., Srimala S., Kaung P., Itoh M., Radzali O. and Fauzi M.N.A. (2010). #Low temperature synthesis of $MgFe_2O_4$ soft ferrite nanocrystallites.# *J. Aust. Ceramic Society,* 46, 11-14.

35. Wyrzykowski D., Hebanowska E., Wiczk G.N., Makowski M. and Chmurzynski L. (2011). #Thermal behaviour of citric acid and isomeric aconitic acids.# *J. Thermal Analysis Calorimetry,* 104(2), 731-735.

36. Preet S. Pandey S.K., Saini N., Koul A. and Rishi P. (2015). #Nisin augments doxorubicin permeabilization and ameliorates signaling cascade during skin carcinogenesis.# *Transl Med.,* 6, 161.

37. Prashant C., Dipak M., Yang C.T., Chuang K.H., Jun D. and Feng S.S. (2010). #Superparamagnetic iron oxide loaded poly (lactic acid)-D-a-tocopherol polyethylene glycol 1000 succinate copolymer nanoparticles as MRI contrast agent.# *Biomater.,* 31(21), 5588-5597.

38. Franco V., Conde C.F. and Conde A. (2005). #Relationship between coercivity and magnetic moment of superparamagnetic particles with dipolar interaction.# *Phys. Rev. B,* 72(17), 1-10.

39. Schulz D.L., Sailer R.A. and Caruso A.N. (2008). #Superparamagnetic Transition Metal Iron Oxygen nanoparticles.# U.S. Patent No. 20090194733.

40. Veiseh O., Gunn J.W. and Zhang M. (2010). #Design and fabrication of magnetic nanoparticles for targeted drug delivery and imaging.# *Adv. Drug Deliv. Rev.,* 62(3), 284-304.

41. Rastogi R., Gulati N., Kotnala R.K., Sharma U., Jayasundar R. and Koul V. (2011). #Evaluation of folate conjugated pegylated thermosensitive magnetic nanocomposites for tumor imaging and therapy.# *Colloids Surf. B,* 82(1), 160–167.

42. Mahmoudi M., Sant S., Wang B., Laurent S. and Sen T. (2011). #Superparamagnetic iron oxide nanoparticles (SPIONs): development, surface modification and applications in chemotherapy.# *Adv. Drug Deliv. Rev.,* 63(1), 24-46.